MOLECULAR PHYSICS
2021, VOL. 119, NOS. 17–18, e1966111 (9 pages)
https://doi.org/10.1080/00268976.2021.1966111

Taylor & Francis
Taylor & Francis Group

JÜRGEN TROE SPECIAL ISSUE

Quantum dynamics of a polar rotor acted upon by an electric rectangular pulse of variable duration

Mallikarjun Karra[a], Burkhard Schmidt[b] and Bretislav Friedrich[a]

[a]Fritz-Haber-Institut der Max-Planck-Gesellschaft, Berlin, Germany; [b]Institut für Mathematik, Freie Universität Berlin, Berlin, Germany

ABSTRACT

As demonstrated in our previous work [J. Chem. Phys. **149**, 174109 (2018)], the kinetic energy imparted to a quantum rotor by a non-resonant electromagnetic pulse with a Gaussian temporal profile exhibits quasi-periodic drops as a function of the pulse duration. Herein, we show that this behaviour can be reproduced with a simple waveform, namely a rectangular electric pulse of variable duration, and examine, both numerically and analytically, its causes. Our analysis reveals that the drops result from the oscillating populations that make up the wavepacket created by the pulse and that they are necessarily accompanied by drops in the orientation and by a restoration of the pre-pulse alignment of the rotor. Handy analytic formulae are derived that allow to predict the pulse durations leading to diminished kinetic energy transfer and orientation. Experimental scenarios are discussed where the phenomenon could be utilised or be detrimental.

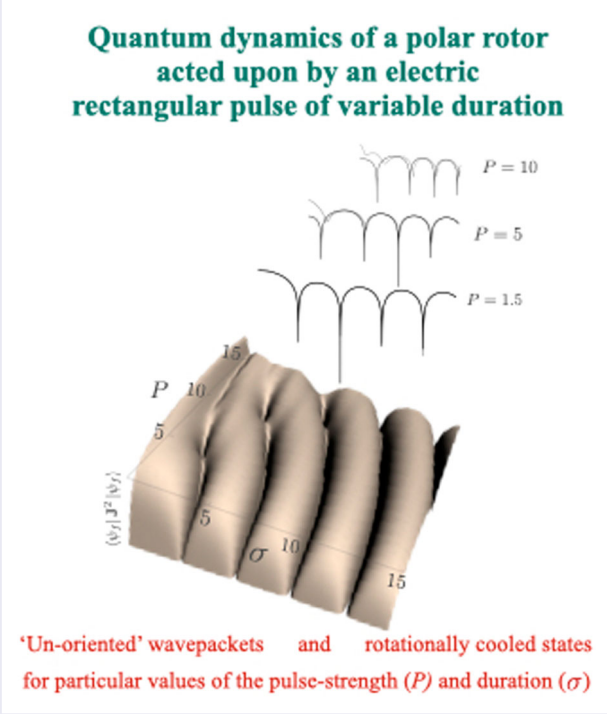

ARTICLE HISTORY
Received 29 April 2021
Accepted 29 July 2021

KEYWORDS
Kicked rotors; orientation and alignment; quantum control

1. Introduction

The ability to manipulate the quantum states of molecular rotors [1,2] has found diverse applications ranging from stereodynamics [3–6] to enantioselectivity [7–9] to coherent control of rotational states [10–15] to quantum information processing [16–20]. Moreover, quantum

CONTACT Bretislav Friedrich bretislav.friedrich@fhi-berlin.mpg.de Fritz-Haber-Institut der Max-Planck-Gesellschaft, Faradayweg 4-6, Berlin D-14195, Germany

rotor dynamics induced by periodic δ-pulses has been linked to quantum chaos, dynamical localisation, and Bloch oscillations [21–25].

Whereas either adiabatic interactions [26–38] or their impulsive, non-adiabatic counterparts [39–53] have received much attention, interactions with finite-duration pulses have been scarce [54–56]. It is the last that are the focus of the present study.

The impulsive interaction of a rotor with a δ-pulse is analytically solvable and represents a benchmark for the behaviour of the expansion (or hybridisation) coefficients of the rotational states, J, that make up the wavepacket created by the pulse. For a purely orienting interaction that arises for a polar rotor acted upon by an electric field, the hybridisation coefficents were found [11,12,56] to be proportional to the spherical Bessel functions of the first kind, $\mathcal{J}_J(P)$, where P is the pulse strength, see below. The zeroes of the hybridisation coefficients, see Figure 1(b) of Ref. [56], determine the minima of the post-pulse populations of the various rotational states and are key to optimising the post-pulse value of a given observable. The figure also illustrates that, typically, many states are hybridised by a δ-pulse. In the same study, we showed that Gaussian pulses of a finite, albeit narrow temporal width much shorter than the rotational period of the rotor, simulate accurately the hybridisation effects of the δ-pulses. However, for longer pulses of small to moderate strength, we observed sudden quasi-periodic drops in the kinetic energy imparted to the rotor by the pulse as a function of the pulse duration, see Figure 4 of Ref. [56].

In the present work we show that the effects of such pulses can be modelled by an even simpler waveform, namely a rectangular electric pulse whose amplitude, ε, is constant over the duration, s, of the pulse, see Figure 1(a). Moreover, we show that the quasi-periodic drops in the imparted kinetic energy are necessarily accompanied by a vanishing orientation and by a restoration of the pre-pulse alignment of the rotor. We identify the origin of the effect in the oscillations in s of the rotor-state populations (hybridisation coefficients) that make up the rotational wavepacket (hybrid). Finally, we provide handy analytic formulae expressed in terms of the characteristics of the pulse and the rotor that allow to predict the pulse durations leading to diminished kinetic energy transfer and orientation and discuss experimental scenarios where this phenomenon could be taken advantage of or be detrimental.

2. A model quantum system

We consider a polar linear rigid rotor with angular momentum $\boldsymbol{J}$ and rotational constant $B = \hbar^2/2I$, with I the moment of inertia, subject to a time-dependent

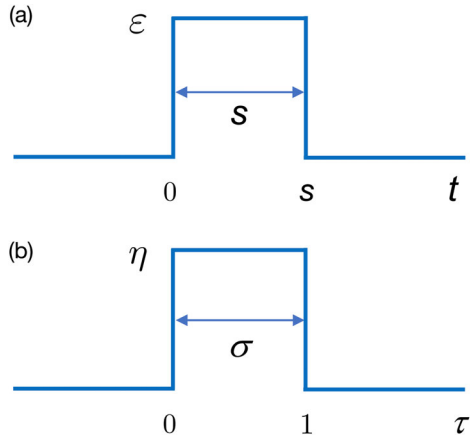

Figure 1. A schematic showing the dependence (a) of the electric field strength ε on time t for a rectangular pulse of duration s and (b) of the orienting parameter $\eta \equiv \mu\varepsilon/B$ on the reduced time τ for a rectangular pulse of duration σ.

potential

$$V(\theta, t) = \begin{Bmatrix} -\mu\varepsilon\cos\theta & 0 \le t \le s \\ 0 & t > s \end{Bmatrix} \qquad (1)$$

with θ the polar angle between the electric field of strength ε and the molecular electric dipole moment of magnitude μ. The potential is nonzero only during time $0 \le t \le s$ and thus corresponds to a rectangular pulse of amplitude $\mu\varepsilon\cos\theta$ and duration s, see also Figure 1(a).

The corresponding time-dependent Schrödinger equation (TDSE)

$$\mathrm{i}\hbar\frac{\partial}{\partial t}|\psi(t)\rangle = \left[B\boldsymbol{J}^2 + V(\theta, t)\right]|\psi(t)\rangle\,, \qquad (2)$$

with $\mathrm{i} = \sqrt{-1}$, can be recast by rescaling time in units of the pulse duration, $\tau \equiv t/s$, as

$$\mathrm{i}\frac{\partial}{\partial \tau}|\psi(\tau)\rangle = \left(\sigma\boldsymbol{J}^2 - \eta\sigma\cos\theta\right)|\psi(\tau)\rangle\,, \qquad (3)$$

where $\sigma = \frac{Bs}{\hbar}$ is the pulse duration in units of the rotational period, $\hbar/B$, and $\eta \equiv \frac{\mu\varepsilon}{B}$ is a dimensionless measure of the orienting interaction. Note that the potential becomes zero for $\tau < 0$ and $\tau > 1$. Integration of the orienting interaction over the pulse duration gives the pulse strength (or kick strength) $P = \int_0^s \frac{\mu\varepsilon}{\hbar}\,\mathrm{d}t = \frac{\mu\varepsilon s}{\hbar} = \eta\sigma$, see also Figure 1(b).

The matrix representation of the Hamiltonian in the free rotor basis set is symmetric tri-diagonal, with matrix elements

$$\langle J', 0|\,\boldsymbol{J}^2\,|J, 0\rangle = J(J+1)\delta_{J',J} \qquad (4)$$

and

$$\langle J',0|\cos\theta\,|J,0\rangle = \sqrt{\frac{J^2}{(2J+1)(2J-1)}}\delta_{J',J-1} + \sqrt{\frac{(J+1)^2}{(2J+3)(2J+1)}}\delta_{J',J+1} \quad (5)$$

We note that well-established perturbative approaches, for example the first-order Magnus expansion, or the time evolution operator of the time-dependent unitary perturbation theory (TDUPT) as developed by Daems *et al.* [57], assume small perturbations and are thus only suitable for treating the σ-dependent effects of our system for $\sigma \ll \sigma\eta$. Furthermore, the potent iterative super-convergent Kolmogorov-Arnold-Moser (KAM) algorithm technique [58,59] is tedious to apply beyond the two-level approximation. Therefore, herein we resort to solving the TDSE numerically by the split-operator method using the Gauss-Jacobi quadrature implemented within the WavePacket software package [60–62]. Apart from that, we set up a ten-level approximation in Mathematica [63] and discuss in detail the two-level approximation valid in the limit of small P.

3. Results and discussion

3.1. Numerical simulations

The numerical simulations presented in this Section have been carried out as a function of the pulse duration σ for a fixed value of the pulse strength $P = \sigma\eta = 1.5$. The range of σ was varied between 0.005 and 10 in steps of 0.005, i.e. from the impulsive, non-adiabatic regime (the results for $\sigma = 0.005$ are in agreement with the theory of δ-kicks [56]) to the adiabatic limit (the results for $\sigma = 10$ approximate well the stationary solutions of the TDSE, Equation (3)). Owing to the rectangular pulse-shape, the present problem may be well treated in a numerically exact way by the diagonalisation of a time-independent Hamiltonian in the (numerically finite) basis of J-states (since quantum number M (= 0) is conserved). We discuss the results for other values of P thus obtained later in Section 3.2.

The results for the initial states $|J_0, 0\rangle$ with $J_0 \in \{0, 1, 2\}$ of the rotor are summarised in Figures 2 and 3. The rotational kinetic energy and the orientation and alignment cosines shown pertain to the state $|\psi_f\rangle$ of the system at the end of the interaction at $\tau = 1$ with a pulse of duration σ and orienting interaction parameter $\eta = \frac{P}{\sigma}$. Expanded in the free rotor basis $|J, 0\rangle$, the post-pulse state is given by

$$|\psi_f\rangle = \sum_J C_J^{J_0}\,|J,0\rangle \quad (6)$$

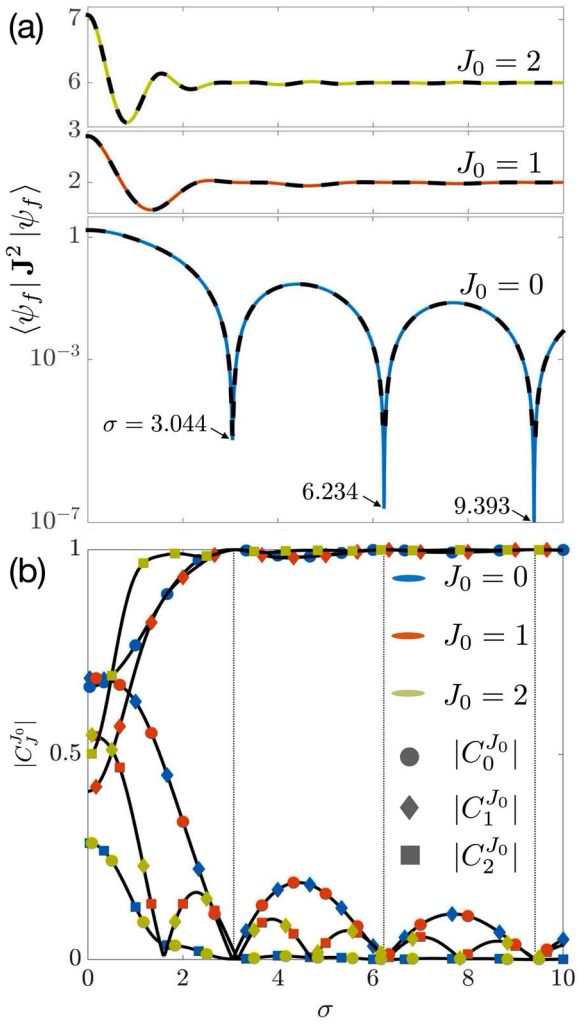

Figure 2. (a) Rotational kinetic energy imparted to a polar rigid rotor in an initial state $|J_0, 0\rangle$ with $J_0 = 0$ (blue), $J_0 = 1$ (red), $J_0 = 2$ (yellow) by a rectangular electric pulse as a function of the pulse duration σ at a fixed pulse strength $P = 1.5$. The dashed black curves represent the kinetic energies obtained from a ten-level approximation presented in Section 3.2. (b) Absolute values of the first three expansion coefficients for each of the three initial states. Note the relationship, $C_j^i = C_i^j$.

where the superscript of the expansion (hybridisation) coefficients, $C_J^{J_0}$, denotes the initial rotational state of the rotor.

Thus the rotational kinetic energy at the end of the pulse becomes

$$\langle\psi_f|\,\boldsymbol{J}^2\,|\psi_f\rangle = \sum_J J(J+1)|C_J|^2 \quad (7)$$

where we dropped the superscript J_0 on C_J for notational simplicity. The dependence of the imparted rotational kinetic energy on the pulse duration, Figure 2(a), exhibits drops that are particularly pronounced for the ground state of the rotor, with $J_0 = 0$, but also appear for the

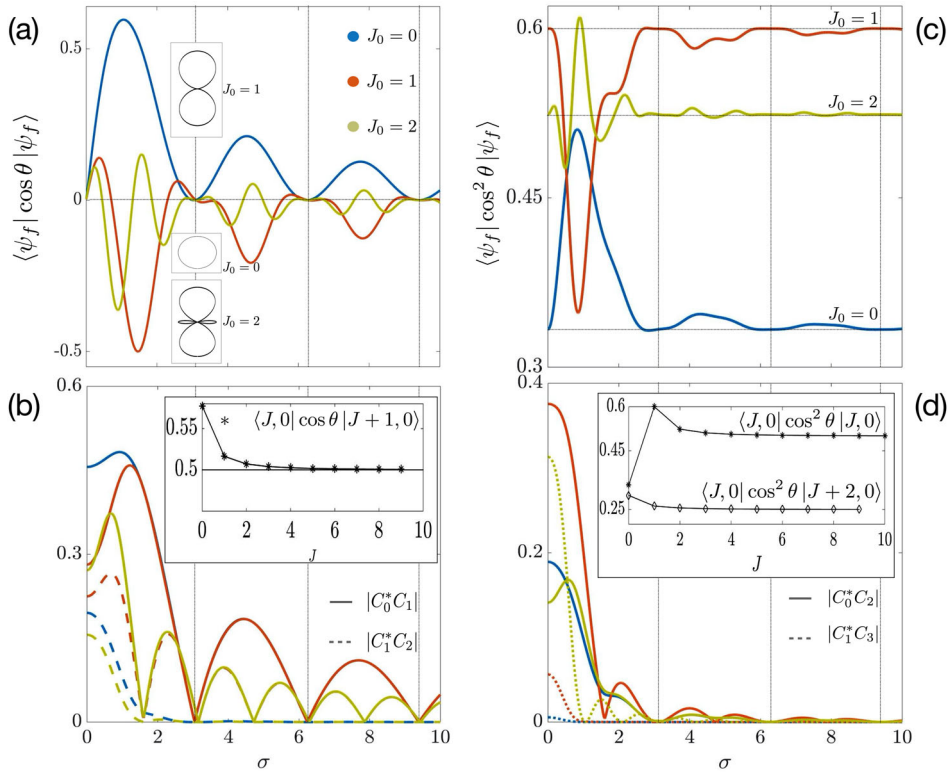

Figure 3. Directional properties of the wavepackets created by a rectangular pulse of pulse strength $P = 1.5$ as a function of the pulse duration σ. (a) Post-pulse orientation cosine for initial rotational states with $J_0 = 0$ (blue), $J_0 = 1$ (red), and $J_0 = 2$ (yellow). The insets show polar plots of the wavefunctions at $\sigma = 3.044$. (b) Absolute values of the products of the coefficients of successive rotational levels. Inset shows the matrix elements of $\cos\theta$ for $\Delta J = \pm 1$, with the first two values evaluating to $\frac{1}{\sqrt{3}}$ and $\frac{2}{\sqrt{15}}$, respectively, such that the large-J limit tends to 0.5. (c) Post-pulse alignment cosine for initial rotational states with $J_0 = 0$ (blue), $J_0 = 1$ (red), and $J_0 = 2$ (yellow). For the case of a large σ (small η), the alignment returns to its initial value. Horizontal lines show the alignment of the field-free states. (d) Absolute values of the products of the coefficients of successive rotational levels with a difference in J of two. Inset shows the matrix elements of $\cos^2\theta$ for $\Delta J = 0, \pm 2$.

higher initial states of the rotor with $J_0 = 1$ and $J_0 = 2$. Figure 2(b) shows the dependence of the corresponding hybridisation coefficients on the pulse duration. A direct consequence of the symmetry of the Hamiltonian H and hence of the propagator $\exp(\frac{\mathrm{i}}{\hbar}Ht)$ is the relationship $C_i^j = C_j^i$, which results in the overlapping of the plot-data indicated by different shapes and colours. The squares of these coefficients, $|C_J|^2$, give the populations of the free rotor basis states in a given wavepacket (hybrid). Close to the adiabatic limit (at $\sigma = 10$), essentially only the initial states are populated after the pulse has passed, i.e. the state of the rotor before and after an adiabatic interaction is the same. This is in sharp contrast with what happens in the impulsive, non-adiabatic regime at short pulses (small σ): a wavepacket is created that is comprised of a number of free-rotor states J whose relative contributions oscillate with a J-dependent frequency as a function of σ. The collective vanishing of the populations of the contributing J states at particular values of σ is thus the apparent cause of the drops in the rotational kinetic energy, cf. Figure 2(a,b). The numerically determined drops occur at $\sigma \approx 3.044, 6.234, 9.393$ for $J_0 = 0$, with a period of a little less than π which, as we will see in Section 3.2, is due to our choice of P.

We note that for the initial state $J_0 = 0$, the kinetic energy ($\approx 2|C_1|^2$) is minimised when the real part of the C_1 coefficient vanishes, i.e. at the three points mentioned above (within the two-state approximation, it does so necessarily due to the sinc prefactor). However, a small imaginary part remains and therefore the kinetic energy does not completely vanish in a large-enough basis. In the case of a weak pulse strength ($P \lesssim 3$), the C_J coefficients with $J \gtrsim 3$ are found to be negligible for $\sigma \gtrsim 2$. One more detail to note is that the starting value of the kinetic energy for $J_0 = 0$ agrees with the energy imparted by an ultrashort pulse ($\frac{2P^2}{3}$) [56].

For higher initial states ($J_0 = 1$ and $J_0 = 2$), the rotational kinetic energy, as a cumulative linear combination of the squares of the coefficients of all populated rotational levels, is found to oscillate in σ with a decaying amplitude from its starting value to the long-pulse

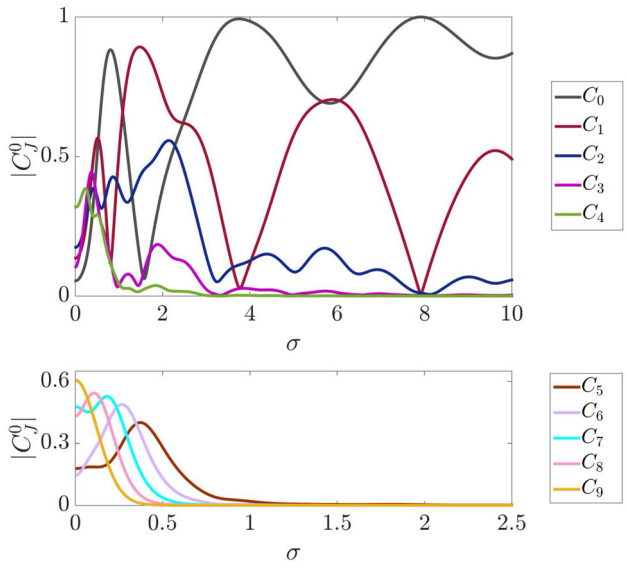

Figure 4. Expansion coefficients for $P = 10$ as a function of the pulse-duration σ as obtained from the ten-level calculation. There is gradual transition with increasing σ to the regime where the two-level model is approximately valid (as seen in the 'bouncing' of the C_1 coefficient).

adiabatic limit, $J_0(J_0+1)$, where only the initial state is populated after the pulse has passed, cf. the upper two curves in Figure 2(a).

The directional properties – the post-pulse orientation and alignment cosines – of the wavepacket created by the rectangular pulse are shown in panels (a) and (c) of Figure 3 as functions of pulse duration σ for a fixed pulse strength $P = 1.5$.

The post-pulse orientation cosine of such a wavepacket is given by

$$\langle\psi_f|\cos\theta\,|\psi_f\rangle = \sum_J C_J^* C_{J+1}\,\langle J,0|\cos\theta\,|J+1,0\rangle + \text{c.c.} \tag{8}$$

where $|\psi_f\rangle$ denotes the final state at the end of the interaction. Owing to the selection rules, the only non-vanishing terms in the expansion are those corresponding to $\Delta J = \pm 1$ see also Equation (5). As seen in Figure 3(a), the orientation cosine vanishes at the values of σ that lead to the drops of the rotational kinetic energy. This behaviour is a consequence of the vanishing of the products of pairs of successive coefficients, see Figure 3(b), that appear in expression (8) for the orientation cosine. The dotted vertical lines affirm that the vanishing of the orientation cosine and of the successive pairs of the hybridisation coefficients indeed occur at the same values of σ. This behaviour is to be expected for any initial state in regions of the $P-\sigma$ space where not-too-many free rotor states are hybridised (see discussion pertaining to Figure 4).

The vanishing of the orientation is visualised in Figure 3(a) by three insets representing the polar plots of the wavefunction for the three different initial states at $\sigma = 3.044$ (the electric field of the pulse is oriented vertically). The near-symmetry of the lobes about the horizontal axis indicates a negligible orientation cosine. However, for the $J_0 = 1$ and $J_0 = 2$ states, the alignment is clearly quite pronounced.

The post-pulse alignment is given by

$$\begin{aligned}\langle\psi_f|\cos^2\theta\,|\psi_f\rangle = &\sum_J |C_J|^2\,\langle J,0|\cos^2\theta\,|J,0\rangle) \\ &+ \sum_J C_J^* C_{J+2}\,\langle J,0|\cos^2\theta\,|J+2,0\rangle \\ &+ \text{c.c.}\end{aligned} \tag{9}$$

with nonvanishing matrix elements arising for $\Delta J = 0, \pm 2$. Figure 3(c) shows the alignment cosine as a function of the pulse duration σ.

The pairwise vanishing of the products of the hybridisation coefficients pertaining to the free rotor states that differ by $\Delta J = \pm 2$ restores the alignment the rotor had in its initial state J_0 for large values of σ. Figure 3(c) demonstrates that particular values of the pulse duration can maximise the alignment. Its degree depends, however, on the pulse strength.

3.2. Two-level approximation

Within the first-order perturbation theory, the probability P_{mk} of a transition from state $|m\rangle$ to state $|n\rangle$ of a two-level quantum system driven by a constant perturbation V is given by $P_{mk} = \frac{V^2t^2}{\hbar}\text{sinc}^2(t\Delta/2\hbar^2)$, where Δ is the energy difference between the two states [64,65]; the sinc function is defined as $\text{sinc}(x) \equiv \frac{\sin x}{x}$. With this in mind, we re-cast Equation (3) explicitly for N rotational levels,

$$\begin{pmatrix}\dot{C}_0(\tau)\\ \dot{C}_1(\tau)\\ \dot{C}_2(\tau)\\ .\\ .\end{pmatrix} = \text{i}\sigma \begin{pmatrix} 0 & \frac{\eta}{\sqrt{3}} & 0 & 0 & 0 \\ \frac{\eta}{\sqrt{3}} & -2 & \frac{2\eta}{\sqrt{15}} & 0 & 0 \\ 0 & \frac{2\eta}{\sqrt{15}} & -6 & . & 0 \\ 0 & 0 & . & . & . \\ 0 & 0 & 0 & . & . \end{pmatrix} \times \begin{pmatrix} C_0(\tau)\\ C_1(\tau)\\ C_2(\tau)\\ .\\ .\end{pmatrix} \tag{10}$$

Table 1. Summary of the eigenproperties of the 2 × 2 Hamiltonian matrices with two different initial populations.

	$\|00\rangle$ and $\|10\rangle$	$\|10\rangle$ and $\|20\rangle$
	$J_0 = 0$	$J_0 = 1$
ξ^{J_0}	$\xi^0 = \sqrt{1+\frac{\eta^2}{3}}$	$\xi^1 = 2\sqrt{1+\frac{\eta^2}{15}}$
$\mathcal{A}^{J_0}_{1,2}$	$\mathcal{A}^0_1 = -\mathcal{A}^0_2 = -\frac{\eta}{2\sqrt{3}\xi^0}$	$\mathcal{A}^1_1 = -\mathcal{A}^1_2 = -\frac{\eta}{\sqrt{15}\xi^1}$
Eigenvalues ($\lambda^{J_0}_{1,2}$)	$\lambda^0_{1,2} = -i\sigma(1 \pm \xi^0)$	$\lambda^1_{1,2} = -i\sigma(4 \pm \xi^1)$
Eigenvectors ($\hat{\boldsymbol{\nu}}^{J_0}_{1,2}$)	$\{\frac{\sqrt{3}}{\eta}(1 \mp \xi^0), 1\}$	$\{\frac{\sqrt{15}}{2\eta}(2 \mp \xi^1), 1\}$

Note: Here ξ^{J_0} is proportional to the argument of the sinc function in Equation (14) and (15) and $\mathcal{A}^{J_0}_{1,2}$ are the initial-state dependent constants of integration.

where the left-hand side is a vector of time derivatives of the expansion coefficients with respect to dimensionless time τ of the N rotational levels.

We now consider the following two-level models formed out of two successive 2 × 2 diagonal sub-blocks of the matrix in Equation (10). A model constructed from the $|0,0\rangle$ and $|1,0\rangle$ states,

$$i\sigma \begin{pmatrix} 0 & \frac{\eta}{\sqrt{3}} \\ \frac{\eta}{\sqrt{3}} & -2 \end{pmatrix} \quad \text{for } J_0 = 0 \tag{11}$$

and a model constructed from the $|1,0\rangle$ and $|2,0\rangle$ states,

$$i\sigma \begin{pmatrix} -2 & \frac{2\eta}{\sqrt{15}} \\ \frac{2\eta}{\sqrt{15}} & -6 \end{pmatrix} \quad \text{for } J_0 = 1 \tag{12}$$

The general solutions for the expansion coefficients constructed from the eigenvalues, λ, and eigenvectors, $\hat{\boldsymbol{\nu}}$, of the matrices are given by the following equation:

$$\mathbf{C}^{J_0}(\tau) = \mathcal{A}^{J_0}_1 \, e^{\lambda^{J_0}_1 \tau} \hat{\boldsymbol{\nu}}^{J_0}_1 + \mathcal{A}^{J_0}_2 \, e^{\lambda^{J_0}_2 \tau} \hat{\boldsymbol{\nu}}^{J_0}_2 \tag{13}$$

where $\mathcal{A}^{J_0}_{1,2}$ are the constants of integration obtained by imposing the initial conditions ($J_0 = 0$ and $J_0 = 1$, respectively). Table 1 summarises the eigenvalues and eigenvectors of the two corresponding block-diagonal sub-matrices.

By substituting $\tau = 1$ into Equation (13), models (11) and (12) render, respectively, the following expressions for the coefficients of the initially unpopulated states,

$$C^0_1(\sigma, P) = \frac{iP \, \mathrm{sinc}(\sigma\xi^0)}{\sqrt{3}} \exp(i\sigma) \tag{14}$$

$$C^1_2(\sigma, P) = \frac{2iP \, \mathrm{sinc}(\sigma\xi^1)}{\sqrt{15}} \exp(4i\sigma) \tag{15}$$

where the argument of the sinc function, ξ^{J_0}, is defined in Table 1; it is proportional to the difference of the two eigenvalues – and thus analogous to the factor $\frac{t\Delta}{2\hbar}$ appearing in the perturbative treatment mentioned above. The zeroes of the sinc function (which coincides with the zeroth-order spherical Bessel function of the first kind, $\mathcal{J}_0$) occur when the argument ξ is an integer multiple of π. Hence for integer n and a pulse strength P, the real-valued roots of the equations

$$\sigma^0_n = \sqrt{\frac{3n^2\pi^2 - P^2}{3}} \approx n\pi \left(1 - \frac{P^2}{6n^2\pi^2}\right) \tag{16}$$

$$\sigma^1_n = \sqrt{\frac{15n^2\pi^2 - 4P^2}{60}} \approx \frac{n\pi}{2} \left(1 - \frac{2P^2}{15n^2\pi^2}\right) \tag{17}$$

yield, respectively, the values of the pulse durations at which the C^0_1 and C^1_2 coefficients vanish. The first-order Taylor expansions of these pulse durations, included in Equations (16) and (17), indicate that the dependence on P of the loci of the zeros of the C^0_1 and C^1_2 coefficients is parabolic. In the weak-perturbation limit, $P \to 0$, the coefficients $C^0_1 (= C^1_0)$ and $C^1_2 (= C^2_1)$ have periods π and $\pi/2$, respectively.

Furthermore, Equations (16) and (17) show that the coefficients C^0_1 and C^1_2 vanish for all positive integer values of n provided the pulse strength satisfies the condition $P \ll \sqrt{3}\pi$ and $P \ll \frac{\sqrt{15}}{2}\pi$, respectively. For larger values of P, we demand $n \geq \frac{P}{\sqrt{3}\pi}$ in order for the solutions σ of Equation (16) to be real-valued. Hence when increasing P, the solutions for low n will disappear one after another. For example, for $P = 10$, this means that $n \geq 2$, as illustrated in Figure 4. A similar argument applies for the solutions of Equation (17).

For integer values of $n = \{1, 2, 3\}$, Equation (16) yields the loci of vanishing C^0_1 at $\sigma^0_1 = \{3.022, 6.224, 9.384\}$ for $P = 1.5$, in close agreement with the values obtained numerically, cf. Figure 2(b). Likewise, from Equation (17) with integer values of $n = \{1, 2, 3, 4\}$, we obtain the loci of the minima of the coefficient C^1_2 at $\sigma^1_2 = \{1.523, 3.113, 4.693, 6.269\}$ for $P = 1.5$, likewise in good agreement with those seen in Figure 2(b).

Figure 4 also illustrates that the behaviour of the expansion coefficients is quite different for stronger perturbations ($P \gtrsim 3$ and small enough values of σ) than for weaker ones. In the short-pulse limit, both the interaction strength $\eta = P/\sigma$ and the nonadiabaticity increase, leading to the hybridisation of higher rotational states. However, their coefficients vanish quicker with increasing σ than those of the lower states. As a result, in this σ regime, the two- or three-level approximation is roughly valid despite a high value of the pulse strength P.

3D views of the post-pulse rotational kinetic energy surface spanned by the pulse parameters P and σ are

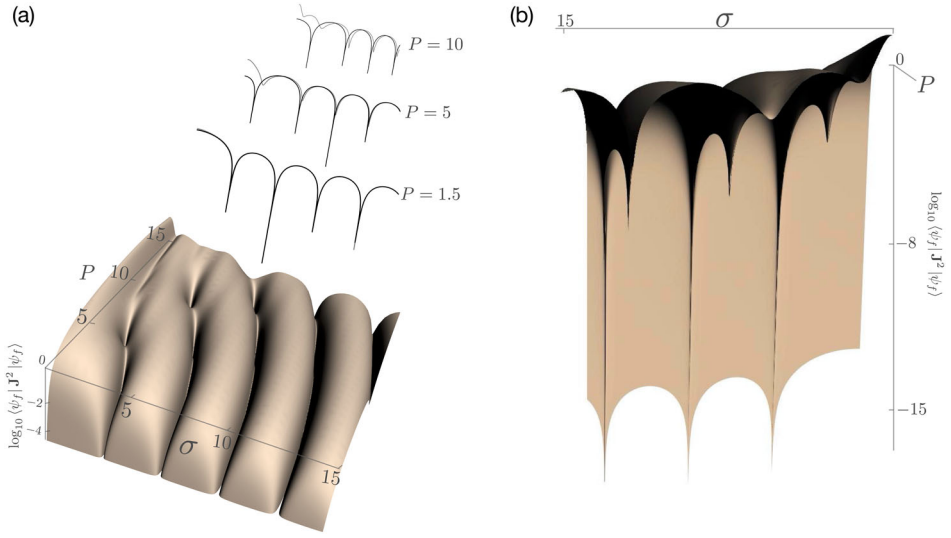

Figure 5. 3D views of the Log_{10}-scaled post-pulse kinetic energy surface for the rotor initially in its ground state. Panel (a) is complemented by a comparison of the calculations of the kinetic energy versus pulse duration curves for fixed values of the pulse strength P as obtained from the two-state model (black) and an accurate numerical calculation (grey). Panel (b) provides a view of the minima of the rotational kinetic energy surface.

shown in Figure 5 for a rotor initially prepared in the ground state $|0,0\rangle$. Panel (a) shows parabolic furrows, cf. Equation (16), consisting of rotationally cooled states with discrete minima along the furrows for specific values of P and σ, cf. Figure 5(b). These discrete minima occur as a result of the coincidence or near-coincidence of the zeroes of multiple coefficients pertaining to different free-rotor states and correspond to maximally cooled hybrid states arising for particular P and σ values. In the absence of closed-form solutions for these coefficients, it is difficult to predict the positions of the minima. However, for the parameter space considered, we find the minima to lie on a family of parallel lines with a slope of 0.577 in the P-σ plane. Therefore, given the position of a minimum, one can predict the approximate location of the other minima from the points of intersection of a given line with the family of parabolae described by Equation (16). Also shown in Figure 5(a) is a comparison of the kinetic energy versus pulse duration curves for fixed values of the pulse strength P as obtained from the two-state model and from an accurate numerical calculation. One can see that for $P < 5$, the two state-model renders the kinetic energy drops quantitatively. The prediction of the two-state model deteriorates at larger P and small σ due the hybridisation of higher states. Nevertheless, the positions of the drops can still be predicted fairly well for sufficiently large σ.

4. Conclusions and prospects

In this work, we have identified the reasons behind the sudden quasi-periodic drops of the kinetic energy of a polar rotor subject to a rectangular electric pulse that occur at specific values of the pulse parameters – its strength P and duration σ. As a corollary, we found that the orientation of the rotor vanishes at the same values of the pulse parameters as the kinetic energy does, independent of the initial state.

Our study has demonstrated that for not-too-high a value of the pulse strength, it is indeed possible to identify a pulse duration at which the expansion (hybridisation) coefficients of the free-rotor states that make up the wavepacket created by the pulse are restricted to just the first few rotational states. An analytic time-dependent two-state model then allowed us to establish a causal connection between the zeros of the hybridisation coefficients, as predicted by the model, and the vanishing of the kinetic energy and orientation.

Current technology makes switching of electrostatic fields at the nanosecond-timescale feasible [66–68]. Thus rectangular electric pulses of a nanosecond duration could be generated and used to control large, slowly rotating molecules with a rotational period of a few tens of nanoseconds. By choosing a proper combination of the pulse strength and pulse duration, isotropic, 'unoriented' wavepackets with vanishing rotational kinetic energy could be created wherever desirable. In this context, for instance, cold chemistry experiments discounting stereoselective enhancement of reaction rates come to mind. Equally importantly, when undesirable, the phenomenon could also be avoided by a proper tuning of the pulse parameters to ensure that the rotor is properly endowed with both kinetic energy and orientation.

We hope that an experiment with cold polar linear rotors with small rotational constants ($B \sim 0.001hc\,\mathrm{cm}^{-1}$ and rotational period ~10 ns) that are subject to rectangular electric pulses will demonstrate the phenomenon studied herein. On the other hand, since we know that full-cycles shorter than the rotational period do indeed result in appreciable changes in orientation (and alignment), smaller rotors with rotational periods in the pico- to femto-second regime could be likewise manipulated by multi-cycle THz pulses [69–71]. The appropriate parameters for suitably shaping a THz pulse for this purpose could be obtained from our numerical simulations.

Future studies will explore the effect for polar polarisable rotors (i.e. with the aligning term, $\propto \cos^2\theta$, included in the potential) as well as for coherently superposed initial states. Moreover, it would be of interest from a mathematical standpoint to explore the connection between the quasi-periodic drops in the kinetic energy and directionality, and the reduction of the error within the second-order TDUPT framework or the iterative superconvergent KAM approach, over the $P-\sigma$ parameter space. A suitable machine-learning algorithm could be employed to 'learn' the rules governing low and acceptable error in the TDUPT, and identify islands in the P-σ parameter space that offer the ability to manipulate a given rotor species. Another avenue to be pursued follows from the observation that a finite-duration pulse is also capable of increasing the kinetic energy (beyond that imparted by an ultrashort non-adiabatic interaction). Amenable to such enhancement of kinetic energy are initial states that are a coherent superposition of several rotational states. This effect could be exploited to generate super-rotors [72].

Acknowledgments

We thank Gerard Meijer for his interest and support, and Marjan Mirahmadi and Jesús Pérez Ríos for fruitful discussions. MK acknowledges support by the IMPRS for Elementary Processes in Physical Chemistry. *We dedicate this paper, with much admiration and our best wishes, to Jürgen Troe on the occasion of his grand jubilee. Among his many contributions to laser chemistry is his work on laser ablation where he made use of fixed fluence to understand the ablation rate at varying pulse lengths* [73].

Disclosure statement

No potential conflict of interest was reported by the author(s).

References

[1] M. Lemeshko, R.V. Krems, J.M. Doyle and S. Kais, Mol. Phys. 111, 1648 (2013). doi:10.1080/00268976.2013.813595.
[2] C.P. Koch, M. Lemeshko and D. Sugny, Rev. Mod. Phys. 91, 035005 (2019). doi:10.1103/RevModPhys.91.035005.
[3] J.J. Larsen, K. Hald, N. Bjerre, H. Stapelfeldt and T. Seideman, Phys. Rev. Lett. 85, 2470 (2000). doi:10.1103/PhysRevLett.85.2470.
[4] J.J. Larsen, I. Wendt-Larsen and H. Stapelfeldt, Phys. Rev. Lett. 83, 1123 (1999). doi:10.1103/PhysRevLett.83.1123.
[5] J.J. Larsen, H. Sakai, C.P. Safvan, I. Wendt-Larsen and H. Stapelfeldt, J. Chem. Phys. 111, 7774 (1999). doi:10.1063/1.480112.
[6] M.H.G. de Miranda, A. Chotia, B. Neyenhuis, D. Wang, G. Quéméner, S. Ospelkaus, J.L. Bohn, J. Ye and D.S. Jin, Nat. Phys. 7, 502 (2011). doi:10.1038/nphys1939.
[7] S. Eibenberger, J. Doyle and D. Patterson, Phys. Rev. Lett. 118, 123002 (2017). doi:10.1103/PhysRevLett.118.123002.
[8] C. Pérez, A.L. Steber, S.R. Domingos, A. Krin, D. Schmitz and M. Schnell, Angew. Chem. Int. Ed. 56, 12512 (2017). doi:10.1002/anie.v56.41.
[9] M. Leibscher, T.F. Giesen and C.P. Koch, J. Chem. Phys. 151, 014302 (2019). doi:10.1063/1.5097406.
[10] Y. Ohshima and H. Hasegawa, Int. Rev. Phys. Chem. 29, 619 (2010). doi:10.1080/0144235X.2010.511769.
[11] I.S. Averbukh, R. Arvieu and M. Leibscher, in *Coherence and Quantum Optics VIII*, edited by N. P. Bigelow, J. H. Eberly, C. R. Stroud, and I. A. Walmsley (Springer US, Boston, MA, 2003), pp. 71–86.
[12] M. Leibscher, I.S. Averbukh, P. Rozmej and R. Arvieu, Phys. Rev. A 69, 032102 (2004). doi:10.1103/PhysRevA.69.032102.
[13] D. Daems, S. Guérin, D. Sugny and H.R. Jauslin, Phys. Rev. Lett. 94, 153003 (2005). doi:10.1103/PhysRevLett.94.153003.
[14] R. Torres, N. Kajumba, J.G. Underwood, J.S. Robinson, S. Baker, J.W.G. Tisch, R. de Nalda, W.A. Bryan, R. Velotta, C. Altucci, I.C.E. Turcu and J.P. Marangos, Phys. Rev. Lett. 98, 203007 (2007). doi:10.1103/PhysRevLett.98.203007.
[15] S. Ospelkaus, K.-K. Ni, G. Quéméner, B. Neyenhuis, D. Wang, M.H.G. de Miranda, J.L. Bohn, J. Ye and D.S. Jin, Phys. Rev. Lett. 104, 030402 (2010). doi:10.1103/PhysRevLett.104.030402.
[16] D. DeMille, Phys. Rev. Lett. 88, 067901 (2002). doi:10.1103/PhysRevLett.88.067901.
[17] E.A. Shapiro, I. Khavkine, M. Spanner and M.Y. Ivanov, Phys. Rev. A 67, 013406 (2003). doi:10.1103/PhysRevA.67.013406.
[18] S. Kotochigova and E. Tiesinga, Phys. Rev. A 73, 041405 (2006). doi:10.1103/PhysRevA.73.041405.
[19] K. Arai and Y. Ohtsuki, Phys. Rev. A 92, 062302 (2015). doi:10.1103/PhysRevA.92.062302.
[20] M. Karra, K. Sharma, B. Friedrich, S. Kais and D. Herschbach, J. Chem. Phys. 144, 094301 (2016). doi:10.1063/1.4942928.
[21] J. Floß and I.S. Averbukh, Phys. Rev. Lett. 113, 043002 (2014). doi:10.1103/PhysRevLett.113.043002.
[22] J. Floß, A. Kamalov, I.S. Averbukh and P.H. Bucksbaum, Phys. Rev. Lett. 115, 203002 (2015). doi:10.1103/PhysRevLett.115.203002.
[23] M. Bitter and V. Milner, Phys. Rev. Lett. 117, 144104 (2016). doi:10.1103/PhysRevLett.117.144104.
[24] M. Bitter and V. Milner, Phys. Rev. Lett. 118, 034101 (2017). doi:10.1103/PhysRevLett.118.034101.

[25] S. Zhdanovich, A.A. Milner, C. Bloomquist, J. Floß, I.S. Averbukh, J.W. Hepburn and V. Milner, Phys. Rev. Lett. 107, 243004 (2011). doi:10.1103/PhysRevLett.107.243004.

[26] B. Friedrich and D.R. Herschbach, Nature 353, 412 (1991). doi:10.1038/353412a0.

[27] J.M. Rost, J.C. Griffin, B. Friedrich and D.R. Herschbach, Phys. Rev. Lett. 68, 1299 (1992). doi:10.1103/PhysRevLett.68.1299.

[28] M.P. Auzinsh and R.S. Ferber, Phys. Rev. Lett. 69, 3463 (1992). doi:10.1103/PhysRevLett.69.3463.

[29] B. Friedrich and D. Herschbach, J. Chem. Phys. 111, 6157 (1999). doi:10.1063/1.479917.

[30] B. Friedrich and D. Herschbach, J. Phys. Chem. A 103, 10280 (1999).doi:10.1021/jp992131w.

[31] B. Schmidt and B. Friedrich, J. Chem. Phys. 140, 064317 (2014). doi:10.1063/1.4864465.

[32] B. Schmidt and B. Friedrich, Phys. Rev. A 91, 022111 (2015). doi:10.1103/PhysRevA.91.022111.

[33] S. Becker, M. Mirahmadi, B. Schmidt, K. Schatz and B. Friedrich, Eur. Phys. J. D 71, 149 (2017). doi:10.1140/epjd/e2017-80134-6.

[34] K. Schatz, B. Friedrich, S. Becker and B. Schmidt, Phys. Rev. A 97, 053417 (2018). doi:10.1103/PhysRevA.97.053417.

[35] B. Schmidt and B. Friedrich, Front. Phys. 2, 37 (2014). doi:10.3389/fphy.2014.00037.

[36] M. Li, A. Petrov, C. Makrides, E. Tiesinga and S. Kotochigova, Phys. Rev. A 95, 063422 (2017). doi:10.1103/PhysRevA.95.063422.

[37] H. Kang, Y. Park, Z.H. Kim and H. Kang, J. Phys. Chem. A 122, 2871 (2018). doi:10.1021/acs.jpca.7b11740.

[38] Y. Park, S. Shin and H. Kang, Acc. Chem. Res. 54, 323 (2021). doi:10.1021/acs.accounts.0c00609.

[39] H. Stapelfeldt and T. Seideman, Rev. Mod. Phys. 75, 543 (2003). doi:10.1103/RevModPhys.75.543.

[40] T. Seideman, Phys. Rev. Lett. 83, 4971 (1999). doi:10.1103/PhysRevLett.83.4971.

[41] L. Cai and B. Friedrich, Collect. Czechoslov. Chem. Commun. 66, 991 (2001). doi:10.1135/cccc20010991.

[42] L. Cai, J. Marango and B. Friedrich, Phys. Rev. Lett. 86, 775 (2001). doi:10.1103/PhysRevLett.86.775.

[43] D. Sugny, A. Keller, O. Atabek, D. Daems, C.M. Dion, S. Guérin and H.R. Jauslin, Phys. Rev. A 71, 063402 (2005). doi:10.1103/PhysRevA.71.063402.

[44] D. Daems, S. Guérin, E. Hertz, H.R. Jauslin, B. Lavorel and O. Faucher, Phys. Rev. Lett. 95, 063005 (2005). doi:10.1103/PhysRevLett.95.063005.

[45] E. Hertz, A. Rouzée, S. Guérin, B. Lavorel and O. Faucher, Phys. Rev. A 75, 031403 (2007). doi:10.1103/PhysRevA.75.031403.

[46] E. Hertz, D. Daems, S. Guérin, H.R. Jauslin, B. Lavorel and O. Faucher, Phys. Rev. A 76, 043423 (2007). doi:10.1103/PhysRevA.76.043423.

[47] S. Guérin, A. Rouzée and E. Hertz, Phys. Rev. A 77, 041404 (2008). doi:10.1103/PhysRevA.77.041404.

[48] N. Owschimikow, B. Schmidt and N. Schwentner, Phys. Rev. A 80, 053409 (2009). doi:10.1103/PhysRevA.80.053409.

[49] N. Owschimikow, B. Schmidt and N. Schwentner, Phys. Chem. Chem. Phys. 13, 8671 (2011). doi:10.1039/c0cp02260h.

[50] S. Fleischer, Y. Khodorkovsky, E. Gershnabel, Y. Prior and I.S. Averbukh, Isr. J. Chem. 52, 414 (2012). doi:10.1002/ijch.201100161.

[51] K. Hamraoui, P. Babilotte, F. Billard, E. Hertz, O. Faucher, L.H. Coudert, D. Sugny and B. Lavorel, Phys. Rev. A 96, 043416 (2017). doi:10.1103/PhysRevA.96.043416.

[52] R. Tehini, K. Hamraoui and D. Sugny, Phys. Rev. A 99, 033419 (2019). doi:10.1103/PhysRevA.99.033419.

[53] V.V. Nautiyal, S. Devi, A. Tyagi, B. Vidhani, A. Maan and V. Prasad, Spectrochim. Acta A Mol. Biomol. Spectrosc. 256, 119663 (2021). doi:10.1016/j.saa.2021.119663.

[54] C. Dion, A. Keller and O. Atabek, Eur. Phys. J. D 14, 249 (2001). doi:10.1007/s100530170223.

[55] J. Ortigoso, M. Rodríguez, M. Gupta and B. Friedrich, J. Chem. Phys. 110, 3870 (1999). doi:10.1063/1.478241.

[56] M. Mirahmadi, B. Schmidt, M. Karra and B. Friedrich, J. Chem. Phys. 149, 174109 (2018). doi:10.1063/1.5051591.

[57] D. Sugny, A. Keller, O. Atabek, D. Daems, S. Guérin and H.R. Jauslin, Phys. Rev. A 69, 043407 (2004). doi:10.1103/PhysRevA.69.043407.

[58] W. Dittrich and M. Reutera, in *Classical and Quantum Dynamics: From Classical Paths to Path Integrals* (Springer Berlin Heidelberg, Berlin, Heidelberg, 2001), pp. 155–162.

[59] D. Daems, A. Keller, S. Guérin, H.R. Jauslin and O. Atabek, Phys. Rev. A 67, 052505 (2003). doi:10.1103/PhysRevA.67.052505.

[60] B. Schmidt and U. Lorenz, Comput. Phys. Commun. 213, 223 (2017). doi:10.1016/j.cpc.2016.12.007.

[61] B. Schmidt and C. Hartmann, Comput. Phys. Commun. 228, 229 (2018). doi:10.1016/j.cpc.2018.02.022.

[62] B. Schmidt, R. Klein and L. Cancissu Araujo, J. Comput. Chem. 40, 2677 (2019). doi:10.1002/jcc.v40.30.

[63] Wolfram Research, Inc., Mathematica, Version 12.2. (Champaign, IL, 2020).

[64] C. Cohen-Tannoudji, B. Diu and F. Laloë, *Quantum Mechanics*, Vol. 1 (Wiley, Weinheim, 1977).

[65] J.J. Sakurai and S.F.E. Tuan, *Modern Quantum Mechanics – Revised Edition* (Addison-Wesley Publishing Company, New York, NY, 1994).

[66] S.Y.T. van de Meerakker, H.L. Bethlem, N. Vanhaecke and G. Meijer, Chem. Rev. 112, 4828 (2012). doi:10.1021/cr200349r.

[67] M. Reberšek and P.D. Miklavčič, Automatika 52, 12 (2011). doi:10.1080/00051144.2011.11828399.

[68] H.J. Lee, T. Shimizu, H. Funakubo, Y. Imai, O. Sakata, S.H. Hwang, T.Y. Kim, C. Yoon, C. Dai, L.Q. Chen, S.Y. Lee and J.Y. Jo, Phys. Rev. Lett. 123, 217601 (2019). doi:10.1103/PhysRevLett.123.217601.

[69] Y. Gao, T. Drake, Z. Chen and M.F. DeCamp, Opt. Lett. 33, 2776 (2008). doi:10.1364/OL.33.002776.

[70] M.V. Arkhipov, R.M. Arkhipov, A.V. Pakhomov, I.V. Babushkin, A. Demircan, U. Morgner and N.N. Rosanov, Opt. Lett. 42, 2189 (2017). doi:10.1364/OL.42.002189.

[71] H.-C. Wu and J. Meyer-ter Vehn, Nat. Photonics. 6, 304 (2012). doi:10.1038/nphoton.2012.76.

[72] I.O. Antonov, P.R. Stollenwerk, S. Venkataramanababu, A.P. de Lima Batista, A.G.S. de Oliveira-Filho and B.C. Odom, Nat. Commun. 12, 2201 (2021). doi:10.1038/s41467-021-22342-6.

[73] F. Beinhorn, J. Ihlemann, K. Luther and J. Troe, Appl. Phys. A 79, 869 (2004). doi:10.1007/s00339-004-2587-0.